Talanta 235 (2021) 122812

Contents lists available at ScienceDirect

Talanta

journal homepage: www.elsevier.com/locate/talanta

# Classification and biomarker identification of prostate tissue from TRAMP mice with hyperpolarized $^{13}$C-SIRA

Anne B. Frahm [a], Deborah Hill [b], Sotirios Katsikis [a], Trygve Andreassen [b], Jan Henrik Ardenkjær-Larsen [a], Tone Frost Bathen [b], Siver Andreas Moestue [b,c], Pernille Rose Jensen [a], Mathilde Hauge Lerche [a,*]

[a] Center for Hyperpolarization in Magnetic Resonance, Department of Health Technology, Ørsteds plads 349, 2800, Kongens Lyngby, Denmark
[b] Department of Circulation and Medical Imaging, Norwegian University of Science and Technology, Trondheim, Norway
[c] Department of Pharmacy, Nord University, Bodø, Norway

ARTICLE INFO

*Keywords:*
Dissolution dynamic nuclear polarization
Prostate cancer
Support vector machines
Random forest
Stable isotope resolved analysis
Isotopic fingerprinting

ABSTRACT

Hyperpolarized $^{13}$C isotope resolved spectroscopy boosts NMR signal intensity, which improves signal detection and allows metabolic fluxes to be analyzed. Such hyperpolarized flux data may offer new approaches to tissue classification and biomarker identification that could be translated *in vivo*.

Here we used hyperpolarized stable isotope resolved analysis (SIRA) to measure metabolite specific $^{13}$C isotopic enrichments in the central carbon metabolism of mouse prostate. Prostate and tumor tissue samples were acquired from transgenic adenocarcinomas of the mouse prostate (TRAMP) mice. Before euthanasia, mice were injected with [U–$^{13}$C]glucose intraperitoneally (i.p.). Polar metabolite extracts were prepared, and hyperpolarized 1D-$^{13}$C NMR spectra were obtained from normal prostate (n = 19) and cancer tissue (n = 19) samples. Binary classification and feature analysis was performed to make a separation model and to investigate differences between samples originating from normal and cancerous prostate tissue, respectively.

Hyperpolarized experiments were carried out according to a standardized protocol, which showed a high repeatability (CV = 15%) and an average linewidth in the 1D-$^{13}$C NMR spectra of 2 ± 0.5 Hz. The resolution of the hyperpolarized 1D-$^{13}$C spectra was high with little signal overlap in the carbonyl region and metabolite identification was easily accomplished. A discrimination with 95% success rate could be made between samples originating from TRAMP mice prostate and tumor tissue based on isotopomers from uniquely identified metabolites.

Hyperpolarized $^{13}$C-SIRA allowed detailed metabolic information to be obtained from tissue specimens. The positional information of $^{13}$C isotopic enrichments lead to easily interpreted features responsible for high predictive classification of tissue types. This analytical approach has matured, and the robust experimental protocols currently available allow systematic tracking of metabolite flux *ex vivo*.

## 1. Introduction

For studies of metabolic activity in intact biological systems, tracking of metabolites originating from isotopically enriched tracer molecules has been the method of choice for decades. Such isotopic profiling has been applied *in vivo* to interrogate dynamic activities of metabolic pathways [1–3] and to evaluate contributions of individual enzymatic reactions to production or consumption of specific metabolites [4,5]. Biological interpretations are supported by the isotopic patterns contributing to group discrimination [6]. In particular, isotopic profiling studies take advantage of unsupervised, multivariate statistical classification (such as principal component analyses) to discriminate strains or conditions based on $^{13}$C-labeling data, without a priori knowledge of the metabolic system [7,8].

Metabolic activity can be quantitatively studied with nuclear magnetic resonance (NMR). By performing NMR in conjunction with $^{13}$C-isotope enriched tracers, specific metabolic pathways can be investigated [9,10]. In recent years real-time analysis of metabolic flux in intact cells and whole organisms has become possible with magnetic resonance spectroscopy (MRS) developed in conjunction with

* Corresponding author.
*E-mail address:* mhauler@dtu.dk (M.H. Lerche).

https://doi.org/10.1016/j.talanta.2021.122812
Received 26 April 2021; Received in revised form 14 August 2021; Accepted 16 August 2021
Available online 20 August 2021

hyperpolarization of $^{13}C$ enriched tracers. Such hyperpolarized $^{13}C$ metabolic MRS tracers enable non-invasive monitoring of tumor progression [11] and cancer treatment efficacy [12]. In particular, hyperpolarization of $^{13}C$ isotopic labelled pyruvate provides a sensitivity boost that allows its metabolic transformation to be followed *in vivo* in humans after an intravenous injection of this molecule [13,14]. In humans, this technology has currently only been clinically approved for a single substrate ($^{13}C$ pyruvate), however, biomarker identification is likely to push for clinical approval of additional substrates [15].

Identification of biomarkers in biological samples is a major challenge that is addressed by metabolomics [16]. The vast majority of NMR metabolomics studies use $^{1}H$ for quantitative high throughput analysis. This is due to a high sensitivity of $^{1}H$ NMR owing to the large gyromagnetic ratio of $^{1}H$, as well as its abundance in biological tissues. The detection limit of $^{1}H$ NMR is in the order of μM concentrations and furthermore it has shown high reproducibility and specificity [17]. In biomarker studies, however, the benefits of $^{1}H$ NMR are compromised by severe signal overlap due to a narrow chemical shift scale and couplings. The main challenge is to identify relevant and related signals amongst a background of complex biology that results in overlapped spectral patterns. Great efforts have been devoted to address this challenge, including the development of dedicated 1D and 2D NMR methods combined with databases, as well as statistical methods based on correlations or ratio analysis [18]. Also, recently, sensitivity enhancement with hyperpolarization techniques have allowed direct detection of nuclei such as $^{13}C$ and $^{15}N$ in metabolite extracts [19–22]. These methods exploit the much larger chemical shift dispersion of nuclei with low gyromagnetic ratios to resolve individual metabolite signals.

Combining isotopic labelling with hyperpolarized 1D-$^{13}C$ NMR provides for a highly sensitive, specific, and quantitative method to identify biomarkers in biological systems [23,24]. This method has been named hyperpolarized $^{13}C$-stable isotope resolved analysis ($^{13}C$-SIRA). Comparable results between this *ex vivo* method and the *in vivo* real time flux applications using hyperpolarized $^{13}C$-MRS implies that the discovery of important biomarkers *ex vivo* using $^{13}C$-SIRA could also be regarded as important biomarkers *in vivo*.

Inspired by this possibility, we wanted to evaluate the $^{13}C$-SIRA method for tissue classification and biomarker identification in a relevant model of human disease. With ongoing clinical trials and published studies of real time hyperpolarized $^{13}C$ metabolism in prostate cancer patients [13,25,26] we decided to make the *ex vivo* study in a model of prostate cancer. To this end we chose the transgenic adenocarcinoma of mouse prostate (TRAMP) model, which has gained widespread attention for its ability to mirror disease pathogenesis of the human prostate [27]. TRAMP mice spontaneously develop autochthonous prostate tumors following the onset of puberty [28]. The tumor progression is androgen-driven and developmentally regulated [29] which could challenge a discrimination between tumor and prostate tissue. In addition, the TRAMP model has been used in several real-time metabolic MRS studies [30,31].

In this study, we used the hyperpolarized $^{13}C$-SIRA method on tissue extracts from TRAMP mice administered with isotopic labelled [U–$^{13}C$] glucose by intraperitoneal injection. This resulted in a highly repeatable, fast, easily interpretable, and generally applicable method for extraction of metabolic information from a complicated biological system. Having established the methodology, it was successfully applied to the challenging task of discriminating between normal and cancerous prostate tissue from TRAMP mice. Furthermore, since signals in the hyperpolarized 1D-$^{13}C$ NMR spectrum could easily be identified as belonging to specific metabolites, the features that were responsible for tissue classification could be evaluated and related to reported *in vivo* findings.

## 2. Materials and methods

### 2.1. Materials and ethics

[U–$^{13}C$]glucose (99%) and deuterium oxide (99.9%) was purchased from Sigma-Aldrich.

All other chemicals were the purest grade available from Sigma-Aldrich.

Prostate tissue was collected from TRAMP mice, which were genetically modified from C57BL/6 mice (Jackson Labs, USA) and bred on the same background in NTNU's comparative medicine core facility. The genotype of the mice was confirmed using PCR, and the animals were regularly monitored for general health status. Breeding, daily care, and experimental work were approved by the Norwegian National Animal Research Authority (FOTS ID 11843).

### 2.2. In vivo experiments

Male TRAMP mice selected for the experiments were 24–48 weeks old. The mice were anaesthetized using 1.5%–2.5% isoflurane with a flowrate of 0.5 l/min; 5 to 1 air to oxygen mixture, before intraperitoneal administration of 10 mg/g body weight [U–$^{13}C$]glucose in saline. The mice were kept anaesthetized for 30 min before sacrifice by cervical dislocation and dissection of the prostate tissue. It has previously been reported that prostate cancer in TRAMP mice can be classified into two groups: well-differentiated (WD) and poorly differentiated (PD) [32,33]. WD tumors are histologically similar to low-grade prostate adenocarcinomas in humans, whereas PD tumors resemble carcinomas of neuroendocrine origin [34], which is rarely seen in the clinic. In this project, we chose to study WD tumors as their phenotype resembles the most prevalent human prostate cancer. Prostate lobes were dissected and defined as normal or WD based on a visual examination during dissection, where overall size, irregular shape and discoloration/hypervascularization were the criteria used to identify cancerous tissue. Cancers located in the seminal vesicles were also included in the experiment. Due to a minimum sample weight requirement of 50 mg wet weight for the hyperpolarized $^{13}C$ NMR analysis, normal prostate lobes were combined together to form a single sample, whereas WD samples were large enough to be separated individually.

### 2.3. Tissue metabolite extraction

Perchloric acid ($HClO_4$) extraction was carried out as described previously [35]. Briefly, $HClO_4$ (7% v/v) solution was added in a 1:4 w/v tissue:$HClO_4$ ratio to the frozen tissue that was homogenized using a mortar and pestle (while keeping the tissue-$HClO_4$ sample cold on ice). Soluble metabolites were extracted by centrifugation (10 min, 10,000 rpm, 4 °C). Supernatant was pH neutralized with KOH, centrifuged, and supernatant was freeze-dried. Tissue metabolite extracts were stored at − 80 °C until prepared for nuclear magnetic resonance spectroscopy.

### 2.4. Conventional NMR on tissue metabolite extracts

Lyophilized tissue metabolite extracts for individual samples were dissolved in 250 μl 40 mM deuterated phosphate buffer and 300 μl $D_2O$. The pH was adjusted to 7.90 ± 0.05 with NaOD or sulfuric acid in $D_2O$. The samples were transferred to 5 mm NMR tubes.

$^{1}H$ NMR spectra were recorded at 300 K on a Bruker Avance III 600 MHz (Bruker BioSpin GmbH, Rheinstetten, Germany) spectrometer, equipped with a 5 mm QCI CryoProbe. Samples were analyzed in automation using a SampleJet autosampler and IconNMR running under Topspin 3.5 pl6. One-dimensional nuclear Overhauser effect (NOE) spectra (pulse program "noesygppr1d") were recorded with 64 k data points, 20 ppm spectral width and 128 scans. For residual water suppression, low power (25 Hz) presaturation of the water resonance was applied during relaxation delay (4 s) and mixing time (10 ms). Spectra

were Fourier transformed to 128 k data points using 0.3 Hz line broadening.

Following conventional NMR the samples were transferred to eppendorf tubes and freeze dried before preparation for $^{13}$C-hyperpolarization.

### 2.5. $^{13}$C-hyperpolarization with Dynamic Nuclear Polarization on tissue metabolite extracts

The lyophilized metabolite samples were dissolved in 50 mg of polarization medium (77 mg trityl radical OX063, 1533 mg glycerol-$d_8$, 1085 mg $D_2O$, 35 mg gadoteridol (100 μmol/g)), and 5 μl of HP001 (50 mM, 1.1-bis (hydroxymethyl)-[1–$^{13}$C]cyclopropane)) was added as an internal standard.

DNP was performed at 3.35 T and 1.4 K in a HyperSense polarizer with microwave irradiation at $f_{\mu w} = 94$ GHz and $P_{\mu w} = 100$ mW. Samples were polarized for 90 min.

### 2.6. Hyperpolarized 1D-$^{13}$C NMR of tissue metabolite extracts

All hyperpolarized tissue metabolites samples (38) were washed out of the polarizer with 5 mL of deuterated phosphate buffer (50 mM, pH 7.4), the front of which dissolved the sample (approx. 1.5 ml). An amount (550 ± 10 μL) of the dissolved sample was automatically transferred from the polarizer to an 11.7 T Bruker NMR spectrometer equipped with a cryoprobe for recording of 1D$^{13}$C NMR spectra.

*NMR parameters*: $^{13}$C 1D NMR spectra of hyperpolarized metabolite samples were acquired using an automated trigger signal after sample arrival to the spectrometer and 3 s preacquisition delay. The acquisition time was set at 1.088 s, at 300 K (27 °C) with a 90° pulse. Proton decoupling was applied during acquisition.

*Sample transfer*: A custom-made sample transfer device was designed to work as an add-on to the Hypersense polarizer based on published principles [36], see supp. info. Fig. S5 for details. The following delay settings were used: Pre-acquisition delay of 3s and a stabilization delay of 305 ms. The travel time between the two sensors were experimentally determined (dependent on tube diameter, sample viscosity and transfer pressure) and was in this study observed to be approx. 800 ms. In total the sample transfer time including stabilization was thus approx. 4.1 s.

### 2.7. Quantification of lactate and fructose

Following the method described in reference 23, we calculated a so-called signal loss coefficient (SLC) for lactate-C1 and fructose-C2. Samples were made containing 22.7 μmol HP001, 40.2 μmol 2–$^{13}$C fructose and 8.8 μmol 1–$^{13}$C lactate in polarization medium as described above. The samples (50 mg preparation per sample) were processed as described for dDNP samples and resulted in a dDNP $^{13}$C NMR spectrum of lactate, fructose and HP001. Lactate and fructose signals were integrated and their ratios to HP001 were related to the sample amount ratios to calculate the SLC.

| Compound (Com) | dDNP ratio (Com/HP001) | Sample amount ratio (Com/HP001) | SLC % |
|---|---|---|---|
| Lactate, C1 | 0.395 (exp1), 0.424 (exp2) | 0.387 | **106 ± 5** |
| Fructose, C2 | 1.62 (exp1), 1.64 (exp2) | 1.771 | **92 ± 1** |

The flux was hereafter quantified by relating the signal measured from known amounts (250 nmol) of HP001 in the samples to the average signal of lactate-C1 or fructose-C2 corrected for the SLC's in 19 prostate and 19 tumor samples and referencing to individual sample amounts (mg wet weight tissue) and time (30 min incubation time). The flux was accordingly given as the amount of $^{13}$C produced per mg wet weight tissue per minute.

Sample preparation for precision measurements and metabolite identity verification.

Metabolite samples (10) originating from prostate tissue, redundant and split from samples included in the main study, were dissolved into one batch in 5 ml water. This batch sample was then divided into 10 samples of 500 μl metabolite extract and freeze dried. Of these samples 8 were prepared and hyperpolarized as the samples included in the main study, see above. The remaining samples were used for conventional NMR ($^1$H–$^{13}$C-HSQC and $^1$H–$^{13}$C-HMBC) to aid metabolite identification between overlapping carbonyl signals (between glutamine C1 and aspartate C4 and between glycine C1 and serine C1) and 1D$^{13}$C NMR for a direct sensitivity comparison.

### 2.8. NMR data processing

All spectra were processed in Mnova [37].

*Hyperpolarized 1D-$^{13}$C NMR:* spectra were Fourier transformed to 128 K points with a 64 K points zero filling and 0.3 Hz line broadening, subsequently manually phased, and a Whittaker smoother baseline correction was applied. The spectra were referenced to HP001 at 25.4 ppm (corresponding to lactate C1 at 185.2 ppm).

*Proton NMR:* 1D NOESY spectra were processed with Bruker TopSpin version 4.0.7. The phase was manually corrected. No baseline correction was found to be needed. The spectra were referenced to the TSP peak at 0 ppm in MatLab [38]. An area of interest was set from 0.05 to 10 ppm with the area of the water peak removed (4.59–5.04 ppm). ICOshift (version 3.0) was used to align the spectra [39]. The spectra were autobinned with bin size of 0.02 ppm. Noise filtering was performed by choosing a representative bin with high level noise (5.27–5.29 ppm) and removing all bins with no values higher than the highest value in this noise bin, leaving 298 features in the dataset.

*2D NMR:* The NMR signals were identified as belonging to specific atoms in energy/glycolytic metabolites by consulting available databases [40]. This was done using distinct chemical shifts of carbonyl carbons and by comparing $^{13}$C–$^{13}$C coupling constant pattern with simulations using the NMR analysis tool box in MNova based on the knowledge that all $^{13}$C-labelled metabolite signals are derived from uniformly [U–$^{13}$C]glucose. The assignment for especially glycine and glutamine for which the carbonyl chemical shift is close to serine and aspartate, respectively, were further verified with $^1$H–$^{13}$C HSQC and $^1$H–$^{13}$C HMBC spectra acquired on a sample from the repeatability study.

### 2.9. Data analysis

Data-matrices of hyperpolarized $^{13}$C NMR spectra: Two datasets were created named "full spectrum" and "metabolite spectrum", respectively. Both datasets were made by manually integrating individual NMR signals in the 38 overlaid spectra and normalizing these integrals to sample weight and to the internal reference (HP001) for the individual spectra.

In the "full spectrum" dataset all NMR signals with an SNR above 3.3 were included, except for signals belonging to the polarization medium, deuterated-glycerol and internal standard (HP001) and impurities from these compounds, as identified from a hyperpolarized spectrum of these. In the "metabolite spectrum" dataset ideally only one unique carbon signal from each metabolite was included. Carbon signals with long $T_1$ (non-protonated carbons) were prioritized. Where several isotopomers of the carbon were identified, a carbon signal representing each isotopomer was included.

All multivariate statistical analysis was done with Python [41]. Available at http://www.python.org using algorithms from Scikit-Learn [42] and SciPy [43]. Retrieved from https://scikit-learn.org/and http://www.scipy.org/.

Prior to Principal component analysis (PCA), the data was mean subtracted and scaled to unit variance.

Feature analysis with random forest algorithm (RF).

Random Forest feature ranking was performed with RFs of 600 trees (with gini as impurity measure, no maximum depth), applied to 70% of the randomly picked but stratified so that the ratio of prostate to tumor samples was preserved. Then by shuffling the values in the remaining 30% of data points, a comparison was made between unshuffled and shuffled classification success. This process was repeated 10.000 times over to obtain the importance ranking. No independent testing was done for the RF analysis, and all the data points were included.

Each features importance was calculated as the mean decrease in accuracy when it was shuffled, with the standard error of the mean (SEM) subtracted. A feature was deemed as significantly important if its measured importance was at least 5% of the importance of the highest ranked feature.

Classification with support vector machine algorithm (SVM).

Features found significantly important were mean subtracted and scaled to unit variance before being used as input for a linear SVM analysis. The SVM soft margin parameter (C) was optimized in a grid search, ranging $C = [2^{-5}, 2^{-4} \ldots 2^{5}]$. Leave-one-out cross validation was applied.

## 3. Results and discussion

### 3.1. Isotopic labelling and dissection of prostate tissue from TRAMP mice

#### 3.1.1. Experimental design

A pilot study was performed to evaluate critical parameters in the study design including tracer choice, administration route, incubation time and the possibility to perform thermal NMR and hyperpolarized 1D-$^{13}$C NMR analysis on the same samples. The data from this pilot study is presented in supp. info and Figs. S1–S3.

To probe the central carbon energy metabolism, [U–$^{13}$C]glucose was chosen as a tracer. The short carbon $T_1$s of protonated glucose (0.6–1.2 s, 11.2 T, 37 °C) have previously led to the use of fully deuterated carbon labelled glucose when applied in hyperpolarization studies [44]. The pilot study, however, showed that an automatic transfer of extracted hyperpolarized [U–$^{13}$C]glucose allowed quantification with high precision despite short carbon $T_1$s. The protonated carbon labelled tracer made it possible to collect thermal NMR spectra on the extracted tissue metabolite samples before acquiring hyperpolarized 1D-$^{13}$C NMR spectra. The pilot study also allowed optimizing the amount of metabolic labelling. We injected 300 mg/ml [U–$^{13}$C]glucose intraperitoneal (i.p.) into the abdominal cavity of sedated mice followed by a 30-min waiting time before sacrifice. Mice remained under isoflurane anesthesia during the 30-min waiting time and were euthanized by cervical dislocation prior to tissue collection. This protocol gave a robust isotopic labelling in prostate tissue of high concentration metabolites (lactate, alanine and glutamate). A similar timing profile for i. p. injections in mice has previously been reported [45] and was in accordance with labelling from intravenous injection (i.v.) protocols [46].

#### 3.1.2. Tissue sample collection and characterization

TRAMP mice from a c57BL/6 background (n = 23) with ages varying from 24 to 48 weeks were included in this study. In total, 38 samples were included: 19 from prostates and 19 from tumors. The tumors originated either from the prostate (8 samples) or from the seminal vesicles (11 samples). Tumor bearing mice were identified by palpation. Palpable tumors are reported to be present in 80% of 32 weeks old TRAMP mice, whereas only about 10% have palpable tumors at 22 weeks of age [47]. Similarly, in our study we had few mice with palpable tumors at early age (none before 22 weeks). The ages of the included mice fell into two groups: 22–32 weeks (15 prostate samples and 10 tumor samples) and 36–48 weeks (4 prostate and 9 tumors), Fig. 1A. The tissue sample sizes varied from the smallest tumors (40 mg wet weight) to the largest tumor (>1 g wet weight), Fig. 1B. In order to standardize tissue amounts, all samples above 240 mg were split to obtain at least 120 mg tissue per split sample. There was no apparent correlation between mouse age or tissue weight and tissue grouping, supp. info. Fig. S4. Thus, all samples were treated as belonging to one cohort.

In this study, we chose to study WD tumors due to their more clinically prevalent phenotype. The two PD tumors that were found (in mice of 25 and 26 weeks of age, respectively) were accordingly excluded from the study. Generally, characterization of prostate cancer tissue in TRAMP mice is non-trivial due to the gradual progression from prostate to tumor tissue. We chose to combine tumors found in the prostate and in the seminal vesicles into one group - tumors - partly due to the number of available tumors and partly due to uncertainty in characterization of the tumor origin in two mice. Characteristics of the different types of tissue samples included in the study can be found in Table 1.

#### 3.1.3. Analytical performance of hyperpolarized $^{13}$C-SIRA of tissue extracts

Building on a published protocol for dissolution Dynamic Nuclear Polarization (dDNP) NMR measurement of cell extracts [23], we developed a method for dDNP NMR measurement of tissue extracts. Critical parameters to be improved were identified including sample preparation and sample transfer time between dissolution of hyperpolarized sample and NMR detection. To address the latter, we built a sample transfer system based on published principles [36]. Details on the set-up can be found in supp. info. and Fig. S5.

With this device, sample transfer time between the polarizer and the NMR detection magnet was significantly reduced to 1.10 ± 0.05 s compared to manual transfer (approx. 12s). Once inside the NMR magnet an additional 3s delay was added before data acquisition to stabilize the sample, resulting in a total transfer time of 4.1s. An added benefit of the automated transfer was a 3-fold concentrated sample, see supp. info. and Fig. S6. The spectral quality of a hyperpolarized 1D-$^{13}$C NMR spectrum acquired on an extract from TRAMP prostate is shown in Fig. 2.

A transfer time of 1.1s over a distance of 4 m is good compared to current published protocols for water dissolved samples [22,48]. Further reduction in the waiting time (currently 3s) may be achieved by coating the receiving NMR tube with Hellmanex® (Hellma analytics), which has shown to reduce microbubbles and improve signal line shape [22].

To assess the performance of the improved sample preparation and transfer we performed a repeatability study on the established tissue extract $^{13}$C-SIRA assay. Redundant samples from the main study were

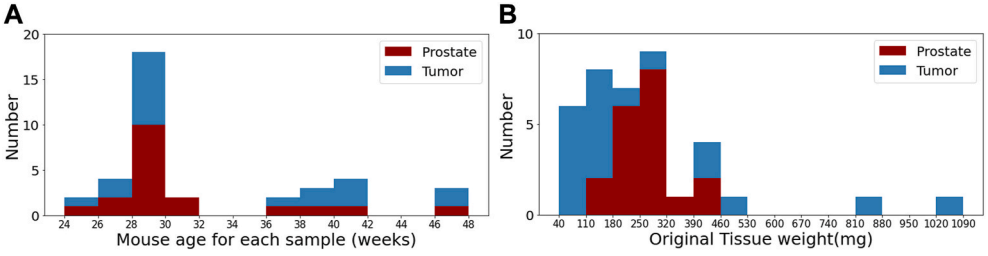


**Fig. 1.** Stacked histogram showing age (A) and weight (B) of the mouse for each sample.

**Table 1**
Characteristics of grouped tissue samples. Variance is given as standard deviations.

| Grouped tissue type | Number of samples | Average mouse age (weeks) | Average received [U–$^{13}$C] glucose dose (ml) | Average original excised tissue size (mg) | Average sample size for hyperpolarized 1D-$^{13}$C NMR (mg) |
|---|---|---|---|---|---|
| Prostate | 19 | 31.4 ± 5.5 | 1.14 ± 0.10 | 271 ± 74 | 149 ± 26 |
| Tumor from prostate | 8 | 33.8 ± 8.1 | 1.16 ± 0.12 | 93 ± 53 | 93 ± 53 |
| Tumor from seminal vesicle | 11 | 34.3 ± 6.7 | 1.14 ± 0.09 | 179 ± 134 | 119 ± 37 |

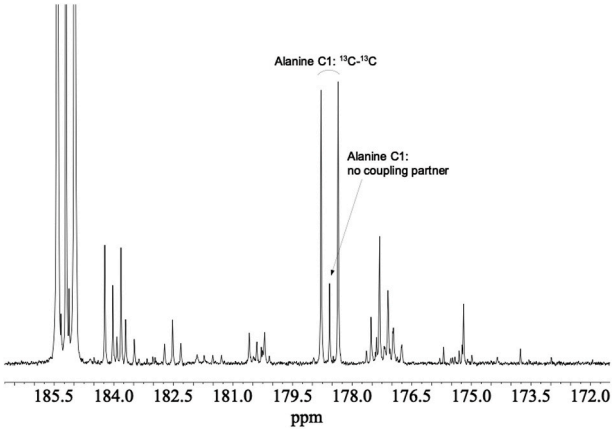


**Fig. 2.** Carbonyl region of hyperpolarized 1D-$^{13}$C NMR spectrum of prostate extract from TRAMP mouse injected i. p. with [U–$^{13}$C]glucose 30 min prior to tissue harvest. A full spectrum is shown in supp. info. Fig. S7. Characteristic isotopomer patterns, highlighted for Alanine C1 as an example, are generally measurable in the spectrum due to a narrow line shape and the large spread of carbon chemical shifts.

pooled and made into identical samples of 135 mg wet tissue each (corresponding to 1 mg dry powder). Samples (8) were prepared for DNP and processed with the established assay. The average precision was CV = 15% for all signals above Limit of Detection (LoD, defined as SNR 3.3). The linewidth of representative signals in the carbonyl region was 2 ± 0.5 Hz. In a previous published study of natural abundance $^{13}$C-spectra of extracts from tomato fruit the precision was higher (CV = 6.4%) when referencing the individual signals to the total $^{13}$C signal [20]. It is possible that the sample concentration taking place during the transfer process resulting in a relatively higher paramagnetic concentration in the final sample is a source of variability. In a future optimization either a reformulation of the polarization matrix to reduce the amount of paramagnetics in the solid-state sample or the addition of a paramagnetic separation step in the transfer could reduce this source of variability.

The polarization in this study has been obtained with direct $^{13}$C DNP. Using an alternative approach where carbon polarization is obtained through cross-polarization from hyperpolarized protons it could be possible to speed up the polarization time in the solid state. This is currently 1.5 h and could be reduced to approx. 30 min using current state of the art cross-polarization equipment [49]. To improve polarization levels further increase in field strength and decrease in temperature are needed. State of the art polarizers provide such conditions whereby a 1.5 times increase in polarization can be obtained [50–52].

### *3.1.4. Classification of tumor and prostate tissue based on isotopic fingerprints*

1D$^{13}$C NMR spectra were acquired from 38 samples hyperpolarized with dDNP. From an initial visual inspection, the spectra originating from prostate and tumor tissue appear very similar (supp. info, Fig. S8). Also, the mean and variance of the three highest metabolite signals did not clearly divide the two types of samples, prompting a more extensive data analysis, Fig. 3.

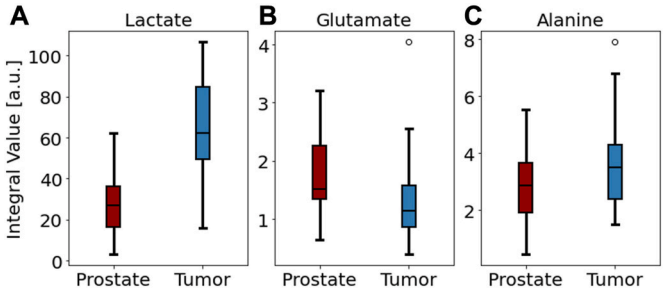


**Fig. 3.** Box plots for high signal metabolites, A) lactate C1, B) glutamate C5 and C) alanine C1. Signal areas were measured as summed integrals over all isotopomers and referenced to the internal standard, HP001. Values are in arbitrary units and represent total integral over the C1 position for lactate and alanine and over C5 for glutamate. The metabolites were identified based on chemical shift and $^{13}$C–$^{13}$C coupling constants.

### *3.1.5. Full spectrum analysis of hyperpolarized 1D-$^{13}$C NMR spectra*

Initially, we wanted to understand whether the hyperpolarized 1D-$^{13}$C NMR spectra as a whole contained sufficient information to separate prostate and tumor samples into the groups they originated from. A dataset was constructed with the measured integral value of all signals above the LoD in the 38 spectra. Peaks that did not originate from the extracted tissue samples were excluded, i.e. the internal standard and signals from the glass former, deuterated glycerol. In total, this amounted to 129 signals, each normalized to the internal standard and the sample weight.

The normalized signal integrals were first subjected to a Principal Component Analysis (PCA). PCA is a commonly used multivariate data analysis technique in metabolomics [17], which transforms the dataset into a lower dimensional set, that can be visualized in a two-dimensional plot. To get an overview of the biological variance in the data and a visual on the separation between prostate and tumor samples, we made a plot of the first two PCA components, Fig. 4A. Point proximity indicates sample similarity. A separation could be seen along both the first-principal component (PC1, explained 36.3% of the variance) and along PC2 (explained 15.6% of the variance) between prostate and tumor samples. The much bigger spread seen within the tumor samples in the PCA is to be expected since biological variability may be high based on the complexity of the TRAMP model, where progression from prostate to tumor metabolism is gradual [29].

To understand if it was possible to make a model that could separate prostate from tumor samples, a binary classification analysis was performed with Support Vector Machines (SVM) as a classifier based on all signals in the hyperpolarized 1D-$^{13}$C NMR spectra. In a previous study, this algorithm proved robust towards small datasets [24]. With the SVM algorithm, a plane was found in the feature-space to maximize the separation between samples belonging to the two classes, prostate or tumor. Prior to the data analysis with SVM we performed a dimensionality reduction by means of feature ranking using the Random Forest (RF) algorithm. Fig. 4B shows the result of the feature ranking of the 129 normalized integrals included in the dataset.

Several signals (34) contributed positively to the discrimination and resulted in a 97% success rate. Of these signals, six had a high relative importance. Performing the discrimination using only the 6 most

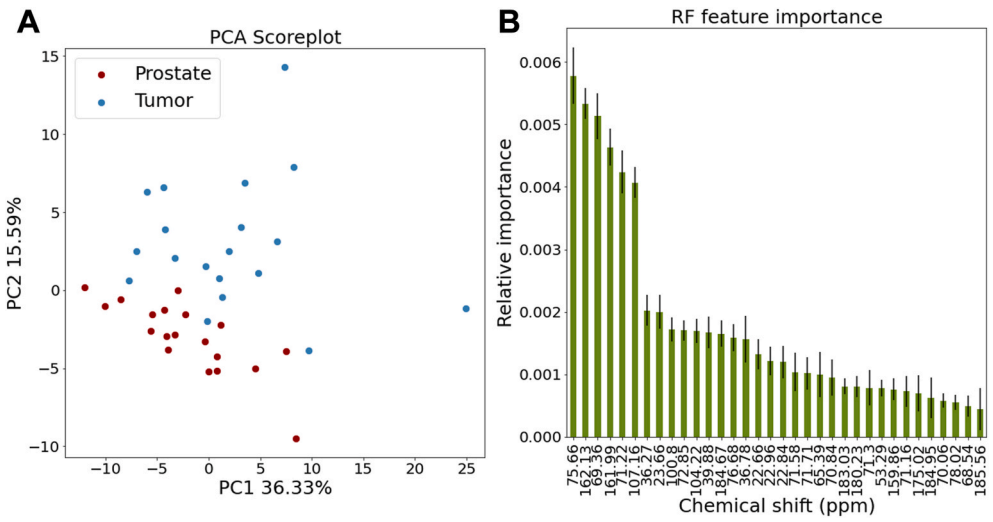


**Fig. 4.** Full spectrum analysis of hyperpolarized 1D-$^{13}$C NMR spectra A) Score plot of PCA. Each point represents a single sample, the coordinates of which are determined by the collective contributions of all sample corresponding signal integrals. Data was mean centered and unit variance scaled before PCA was applied. The PC1 x PC2 plan accounted for 51.9% of total variation among data points. B) Feature ranking performed with the Random Forest (RF) algorithm. 34 signals contributed positively to the discrimination between tumor and prostate tissue, 30 of these are shown). Six signals had a relatively higher importance than the rest.

important signals allowed a discrimination with 95% success rate between tumor and prostate tissue samples.

An inspection of the six signals that allowed a 95% successful discrimination showed that these signals carried little information about metabolites originating from isotopic labelled glucose: Three signals (including two carbamates, 162.1 and 162 ppm) had very low SNR (<5) and were singlets. This indicated that they originated from non-isotopic labelled signals. One additional singlet was not identified (107.2 ppm, SNR<10). The last two signals were from a singlet originating from the lactate C2 isotopomer and from glucose C4α. Although highly valuable as a tool to discriminate between tissue samples with similar origin, this full spectrum analysis without prior knowledge did not provide clear information to be extracted about metabolites originating from the isotope labelled substrate.

Since the most commonly used data type for NMR metabolomics is $^{1}$H NMR data, we chose to cross examine the supervised classification of the tissue samples based on full spectrum hyperpolarized 1D-$^{13}$C NMR with a similar analysis performed with $^{1}$H NMR data collected on the same samples. A full account on the $^{1}$H NMR spectral analysis can be found in supp. info and Fig. S9. The signals in the $^{1}$H NMR spectra were binned into 298 spectral areas (0.02 ppm/bin). In general, the errors in the RF analysis were high, however one bin that included a signal at 7.13 ppm was significantly more important than the rest and an SVM analysis with this feature alone allowed a 97% discrimination. Including additional two bins (signals at 6.81 and 7.11 ppm, respectively) allowed a perfect discrimination of 100%. These chemical shifts suggest that the metabolite behind includes a phenol group, where para-cresol or p-hydroxyacetic acid are likely candidates. Both of these metabolites are bacterially produced and constituents in urine. While these metabolites could separate the two sample groups included in this study, they are not likely to originate from the molecular $^{13}$C-tracer.

### 3.1.6. Isotopic labelled metabolite information and interpretation

To investigate the value of molecular $^{13}$C-tracer related metabolites for discrimination between prostate and tumor tissue, we created a metabolite selective dataset. The resolution of $^{13}$C resonances is much higher than for $^{1}$H due to the large chemical shift range of $^{13}$C (250 ppm vs. 14 ppm) resulting in well separated metabolite signals. The isotopic labelling of metabolites originating from [U–$^{13}$C]glucose further allows biochemically related metabolites to be identified in a background of unlabelled metabolites, which can be two orders of magnitude lower in signal intensity. The uniform isotopic label, if transferred into the metabolite, also results in $^{13}$C–$^{13}$C couplings that, along with the chemical shift of the $^{13}$C signal, generally permit an unambiguous assignment of the signal as belonging to an isotopomer of a specific metabolite. Thus, a metabolite selected dataset could be created using this prior knowledge that allowed direct interpretation of isotopic labelled signals important for classification.

### 3.1.7. Metabolite based analysis of hyperpolarized $^{13}$C-SIRA spectra

A dataset was constructed with integral values of identified metabolite signals from the carbonyl area of the spectra in the 38 included spectra. One carbon position was included per metabolite selected from the carbonyl region representing the longest $T_1$ carbons. For most metabolites both a doublet and a singlet isotopomer were present in the spectrum, Fig. 2. Both isotopomer signals were included with the $^{13}$C–$^{13}$C doublet represented in the dataset by one of its signals. In total this amounted to 35 signals, each normalized to the internal standard and the sample weight.

A plot of the first two PCA components, Fig. 5A, showed less variance between the prostate and tumor group compared to the full spectrum dataset (Fig. 4A.) even though the total explained variance was greater (58.1% vs. 51.9%). It could seem from this group separation that there were two fractions of tumor samples. We thus investigated if the PCA plot could indicate a separation between the tumor samples e.g. into tumors found in the prostate and tumors found in the seminal vesicles, supp. info. Fig. S10. However, the study sample number did not support such separation.

With the supervised model, 12 signals contributed positively to the discrimination. Two signals had a high relative importance as seen from the RF analysis, Fig. 5B. Using only these two features, a discrimination with 92.1% success rate could be obtained, whereas including the 12 highest ranked signals allowed a discrimination with 95% success rate between tumor and prostate tissue sample. This success rate did not increase further by including the remaining 6 signals that showed positive ranking from the RF analysis. The identity of the 12 signals, which allowed a 95% successful discrimination is shown in Table 2.

Whereas metabolites originating from the molecular $^{13}$C-tracer is straightforwardly identified in the hyperpolarized 1D-$^{13}$C NMR spectra it is difficult to make use of such prior knowledge from analysis of $^{1}$H NMR spectra. Administration of [U–$^{13}$C]glucose significantly increase the signal overlap on the narrow $^{1}$H chemical shift scale due to the carbon proton couplings, which at the same time are those that carry the valuable biochemical information. Usually only a few metabolites, such as high concentration metabolites in less crowded spectral regions, e.g. alanine methyl and lactate methyl groups and proton attached to C2 in lactate, can be unambiguously identified and quantified in a $^{1}$H NMR spectra [24,53]. For this reason, we did not attempt to make a comparison to $^{1}$H NMR performance using a dataset where only tracer specific metabolites had been selected.

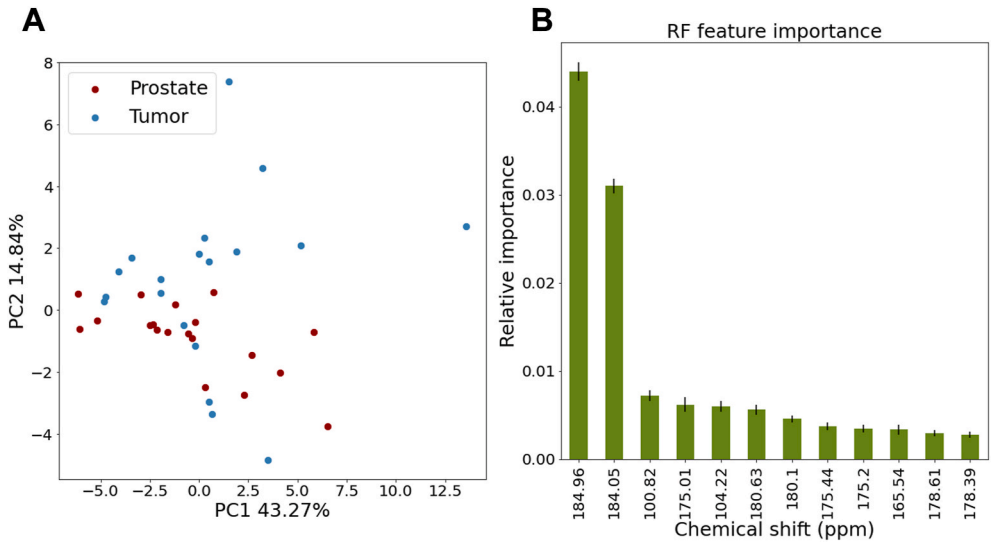


**Fig. 5.** Metabolite analysis of hyperpolarized 1D-$^{13}$C NMR spectra A) Score plot of PCA. Data was mean centered and unit variance scaled before PCA was applied. The PC1 x PC2 plan accounted for 58.1% of total variation among data points. B) Feature ranking performed with the Random Forest (RF) algorithm. 12 signals contributed positively to the discrimination between tumor and prostate tissue. Two signals had a relatively higher importance.

**Table 2**
Identity of 12 features with highest rank in an RF analysis of the metabolite dataset. The score is given as the success rate obtained when including the metabolite and all previous metabolites, i.e. a 92.1 score is obtained when including both lactate C1 and glutamate C5.

| Feature # | RF Ranking | Score (%) | Chemical shift | Identity |
|---|---|---|---|---|
| 1 | 0.044 ± 0.0010 | 81.6 | 184.96 | lactate C1, doublet |
| 2 | 0.031 ± 0.0008 | 92.1 | 184.05 | glutamate C5, singlet |
| 3 | 0.007 ± 0.0006 | 89.5 | 100.82 | beta fructofuranose, singlet |
| 4 | 0.006 ± 0.0008 | 92.1 | 175.01 | serine C1, doublet |
| 5 | 0.006 ± 0.0006 | 92.1 | 104.22 | alfa fructofuranose, singlet |
| 6 | 0.004 ± 0.0006 | 92.1 | 180.63 | glutamine C5, doublet |
| 7 | 0.004 ± 0.0004 | 92.1 | 180.10 | aspartate C1, singlet |
| 8 | 0.003 ± 0.0004 | 92.1 | 175.44 | glycine C1, singlet |
| 9 | 0.003 ± 0.0005 | 92.1 | 175.20 | glycine C1, doublet |
| 10 | 0.003 ± 0.0003 | 92.1 | 165.54 | urea |
| 11 | 0.003 ± 0.0004 | 92.1 | 178.61 | alanine C1, singlet |
| 12 | 0.002 ± 0.0004 | 94.7 | 178.39 | alanine C1, doublet |

Based on previously published results it is expected that only carbonyl carbons in high concentration metabolites such as lactate can be measured with conventional $^{13}$C direct detect NMR [23]. An SNR range in the 38 samples of the 12 signals shown to carry discriminating information is reported in Supp. Infor. Fig. S11a. Also, a direct comparison between a thermal $^{13}$C spectrum of 130 mg mouse prostate tissue with the hyperpolarized spectrum of in identical sample can be found in Supp. Inform. S12. It is clear from this comparison that only the high concentration metabolites (lactate, glutamate and alanine) are detected in the thermal $^{13}$C experiment even after 14 h acquisition time.

### 3.1.8. *Biomarker identification*

In Table 2 it was seen that isotopomers from several metabolites could play a role in the discrimination of prostate and tumor tissue from TRAMP mice. We further investigated their individual and relative contribution to a separation using a PCA loading plot, Fig. 6. The loading plot showed that fructo-furanoses mostly influences PC2. Lactate, aspartate and glutamate have almost equal weight on both components and the remaining metabolites mostly contributes to PC1. Not surprisingly, the two fructo-furanoses have identical impact. The signals from lactate and aspartate are closely and positively related but negatively related to the fructo-furanoses. The rest of the signals relate positively in two groups. Serine and alanine signals in one group and glutamine, glutamate, glycine and urea in another group. A box-plot analysis of these 12 metabolite isotopomers, supp. info. Fig. S11b, showed lactate and serine to be increased in tumor tissue whereas the fructofuranoses, glutamate, glutamine and urea were lower in tumor tissue compared to prostate tissue. A Bonferroni corrected T-test on the 12 selected metabolites showed a difference on a 5% significance level between tumor and prostate samples for lactate, glutamate and serine.

Lactate was expected to contribute to discrimination between prostate and tumor tissue from TRAMP mice. Several metabolic imaging studies of prostate and tumors in TRAMP mice have shown how lactate signal increase with tumor progression [30,31]. Using lactate alone for the discrimination between prostate tissue and WD tumors gave however a success rate (81.6%) similar to what could be obtained by chance for the metabolite dataset (highest score from randomizing tumor and prostate samples was 79%). The success rate could be significantly increased to 92.1% by including at least one of the other 11 features discussed above.

Although not significant in a Pearson correlation the finding that fructose is negatively related to lactate in the discrimination of WD tumor tissue from normal prostate tissue is especially interesting to include in further biomarker investigations. Fructose metabolism is emerging as important in cancer biology, which can be explained by an increased intake of this nutrient in cancers [54]. Although most fructolysis takes place in the liver, both normal prostate cells and prostate cancer cells take up and metabolize fructose. GLUT5 is a specific transporter of fructose and it has been reported to be overexpressed both in normal human prostate and in prostate cancer [55]. The so-called polyol pathway consists of two reversible reactions; using sorbitol as an intermediate it allows conversion of fructose to glucose, or

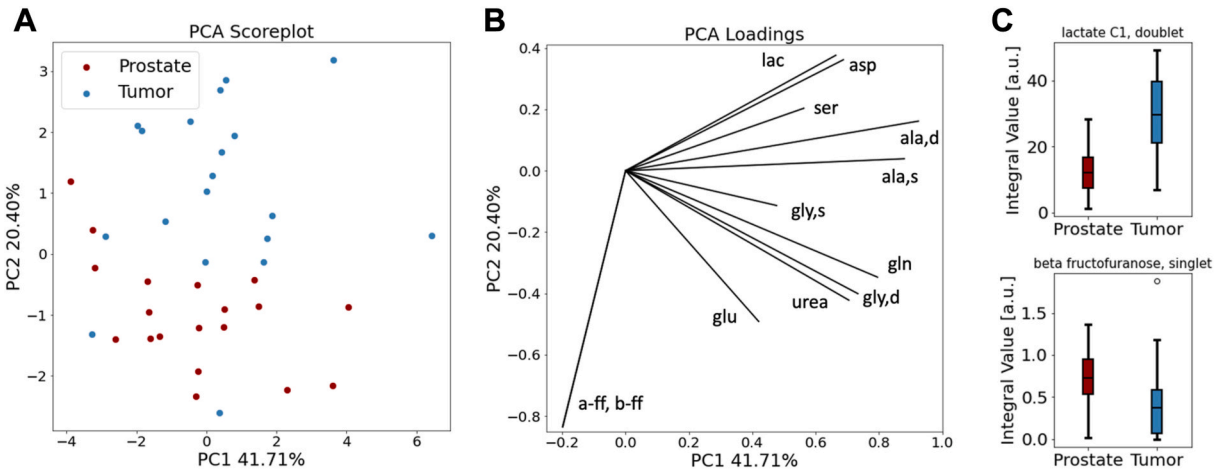


**Fig. 6.** PCA plots using only the 12 RF selected highest ranked features. A. Score plot of PCA. Each point represents a single sample, the coordinates of which are determined by the collective contributions of all sample corresponding signal integrals. Data was mean centered and unit variance scaled before PCA was applied. The PC1 x PC2 plan accounted for 62.11% of total variation among data points. B. Loading plot of PCA. The Impact and correlation of the 12 features listed in Table 2 are shown. Interpretation: Projection of vectors to the respective axes infer their weight on the PCs. Close proximity of vectors, forming a small angle between them, suggest positive correlation between the features whereas vectors meeting at 90° suggests no correlation and vectors with larger angles infer negative correlation. Shorter length vectors suggest less importance (ser and gly,s). Here shown for the PC1 x PC2 plan, why interpretation could be influenced by including more dimensions. C. Box-plot for Lactate and beta fructofuranose. Values are in arbitrary units and represents integral over the specific isotopomer included in the analysis. Box-plot for the remaining 10 high ranking metabolites are shown in supp. info. Fig. S11.

alternatively allows for an endogenous production of fructose from glucose. The latter makes it possible for cells to bypass glycolytic regulation and increase the glycolytic rate [56]. The polyol pathway has been reported as active both in normal prostate and prostate cancer [57]. Fructose is also connected to lipogenesis, which is another important requirement of proliferating cancer cells. The large fructose signal in TRAMP prostate tissue seen in our study could, due to a 30 min circulation time of the molecular $^{13}$C-tracer, result in production of $^{13}$C labelled fructose in the liver rather than directly in the prostate. In that case the difference in fructose signal between the two tissue types would be due to uptake capability rather than production.

It is possible to make the SIRA method quantitative by quantifying the signal loss of individual signals in the transfer between the polarizer and the NMR magnet [23]. Here this was done for lactate and fructose and allowed a quantification of the average flux of $^{13}$C into these two metabolites. The average flux of $^{13}$C into lactate was more than twice in tumor tissue compared to prostate tissue (50 pmol/mg wet weight tumor tissue/min vs. 21 pmol/mg wet weight prostate tissue/min). Fructose flux was expectedly much lower than lactate and showed a reverse dependence of tissue type with a larger flux into prostate tissue (0.6 pmol/mg wet weight tumor tissue/min vs. 1.1 pmol/mg wet weight prostate tissue/min).

Hyperpolarized $^{13}$C-fructose has already been developed as a real time metabolic imaging marker and tested in TRAMP mice for spectroscopic imaging of PD tumors [58]. With an improved understanding of fructolysis in different stages of the prostate cancer development it is likely that a biomarker could be developed with a combination of $^{13}$C-pyruvate and $^{13}$C-fructose. Such combined tracer would target lactate derived from pyruvate and fructose metabolism simultaneously and thus potentially improve the diagnostic accuracy of prostate cancer compared to focusing solely on $^{13}$C-lactate derived from pyruvate.

Several of the other identified metabolites shown to carry discriminative information could potentially be important in the development of new hyperpolarized biomarkers. In particularly the multiple roles of glutamine in cancer could be utilized with its increased uptake and conversion to glutamate, which is important for protection against oxidative damage [59]. Hyperpolarized glutamine has also previously been shown to probe treatment response in prostate cancer cells [60]. Also, an increased amino acid synthesis to provide building blocks for prostate cancer proliferation may be probed with labelling of serine and glycine possibly through administration of hyperpolarized trioses [61] or with labelling of alanine from hyperpolarized pyruvate [30].

## 4. Conclusion

In this study, we used the hyperpolarized $^{13}$C-SIRA method to collect 1D-$^{13}$C NMR data on normal and cancerous prostate tissue extracts from TRAMP mice administered with isotopic labelled [U–$^{13}$C]glucose.

With a combination of a random forest algorithm applied to evaluate signal importance and support vector machines for classification it was possible to make a discrimination with 95% success rate between tumor and normal prostate tissue.

Signals in the hyperpolarized 1D-$^{13}$C NMR spectrum could easily be assigned to specific metabolites. The signals that were responsible for tissue classification could be evaluated and related to reported *in vivo* findings. In particular, the evaluation suggested that targeting pyruvate and fructose metabolism in combination could provide additional information compared to pyruvate alone for prostate cancer diagnosis.

## Declaration of competing interest

The authors declare that they have no known competing financial interests or personal relationships that could have appeared to influence the work reported in this paper.

## Acknowledgements

The authors gratefully acknowledge funding by the Danish National Research Foundation (Grant DNRF124).

Hyperpolarized 1D-$^{13}$C NMR data in this study was acquired with equipment partially funded by the Novo Nordisk Foundation (NNF19OC0055825).

The tissue extraction procedures and $^{1}$H -NMR experiments were performed at the MR Core Facility, Norwegian University of Science and Technology (NTNU). MR core facility is funded by the Faculty of Medicine and Health Sciences at NTNU and Central Norway Regional Health Authority.

TRAMP mice breeding, housing, and genotyping was provided by the Comparative medicine Core Facility (CoMed), Norwegian University of Science and Technology (NTNU). CoMed is funded by the Faculty of

Medicine at NTNU and Central Norway Regional Health Authority.

The NMR center at DTU is acknowledged for the high-resolution $^{1}H$–$^{13}C$ HSQC and HMBC Spectrum acquired on their 800 MHz Avance II NMR spectrometer.

Anne B. Frahm was supported by a travel and study grant from the Danish Cancer Society for a visiting stay at NTNU (Grant R235-A14222-19-S44).

## Appendix A. Supplementary data

Supplementary data to this article can be found online at https://doi.org/10.1016/j.talanta.2021.122812.

## Credit author statement

Conceptualization, D.H. S.A.M P.R.J A.B.F. and M.H.L; Animal and tissue methodology, D.H. S.A.M. A.B.F.; NMR methodology, T.A.; dDNP NMR methodology, A.B.F. and S.K.; Statistical modelling, A.B.F; data analysis, A.B.F. P.R.J. and M.H.L.; Study evaluation and data discussion, D.H. S.A.M. P.R.J A.B.F T.A. T.F.B and M.H.L.; original draft preparation, M.H.L.; review and editing, D.H. S.A.M. P.R.J A.B.F T.A. S.K T.F.B J-H.A-L. and M.H.L; All authors have read and agreed to the published version of the manuscript.

## References

[1] T.W.M. Fan, A.N. Lane, R.M. Higashi, M.A. Farag, H. Gao, M. Bousamra, D. M. Miller, Altered regulation of metabolic pathways in human lung cancer discerned by $^{13}C$ stable isotope-resolved metabolomics (SIRM), Mol. Canc. 8 (2009) 41–60, https://doi.org/10.1186/1476-4598-8-41.

[2] E.A. Maher, I. Marin-Valencia, R.M. bachoo, T. Mashimo, J. Raisanen, K. J. Hatanpaa, A. Jindal, F.M. Jeffrey, C. Choi, C. Madden, D. Mathews, J.M. Pascual, B.E. Mickey, C.R. Malloy, R.J. DeBerardinis, Metabolism of [U-$^{13}C$]glucose in human brain tumors in vivo, NMR Biomed. 25 (11) (2012) 1234–1244, https://doi.org/10.1002/nbm.2794.

[3] C.T. Hensley, B. Faubert, Q. Yuan, N. Lev-Cohain, E. Jin, J. Kim, L. Jiang, B. Ko, R. Skelton, L. Loudat, M. Wodzak, C. Klimko, E. McMillan, Y. Butt, M. Ni, D. Oliver, J. Torrealba, C.R. Malloy, K. Kernstine, R.E. Lenkinski, R.J. DeBerardinis, Metabolic heterogeneity in human lung tumors, Cell 164 (2016) 681–694, https://doi.org/10.1016/j.cell.2015.12.034.

[4] A.L. Holleran, G. Fiskum, J.K. Kelleher, Quantitative analysis of acetoacetate AS-30D hepatoma cells with $_{13C\ and}$ metabolism in 14C isotopic techniques, American J. Physiol-endocrinol and Metab. 272 (6) (1997) E945–E951, https://doi.org/10.1152/ajpendo.1997.272.6.E945.

[5] S.C. Burgess, T.T. He, Z. Yan, J. Lindner, A.D. Sherry, C.R. Malloy, J.D. Browning, M.A. Magnuson, Cytosolic phosphoenolpyruvate carboxykinase does not solely control the rate of hepatic gluconeogenesis in the intact mouse liver, Cell Metabol. 5 (4) (2007) 313–320, https://doi.org/10.1016/j.cmet.2007.03.004.

[6] S. Heux, C. Bergés, P. Millard, J.-C. Portais, F. Létisse, Recent advances in high-throughput $^{13}C$-fluxomics, Curr. Opin. Biotechnol. 43 (2017) 104–109, https://doi.org/10.1016/j.copbio.2016.10.010.

[7] N. Zamboni, U. Sauer, Model-independent fluxome profiling from $^{2}H$ and $^{13}C$ experiments for metabolic variant discrimination, Genome Biol. 5 (2004) R99, https://doi.org/10.1186/gb-2004-5-12-r99.

[8] S. Heux, J. Poinot, S. Massou, S. Sokol, J.-C. Portais, A novel platform for automated high-throughput fluxome profiling of metabolic variants, Metab. Eng. 25 (2014) 8–19, https://doi.org/10.1016/j.ymben.2014.06.001.

[9] A.N. Lane, J. Tan, Y. Wang, J. Yan, R.M. Higashi, T.W.M. Fan, Probing the metabolic phenotype of breast cancer cells by multiple tracer stable isotope resolved metabolomics, Metab. Eng. 43 (2017) 125–136, https://doi.org/10.1016/j.ymben.2017.01.010.

[10] P. Giraudeau, NMR-based metabolomics and fluxomics: developments and future prospects, Analyst 145 (2020) 2457, https://doi.org/10.1039/D0AN00142B.

[11] P.J. Shin, Z. Zhu, R. Camarda, R.A. Bok, A.Y. Zhou, J. Kurhanewicz, A. Goga, D. B. Vigneron, Cancer recurrence monitoring using hyperpolarized [1-$^{13}C$]pyruvate metabolic imaging in murine breast cancer model, Magn. Reson. Imag. 43 (2017) 105–109, https://doi.org/10.1016/j.mri.2017.07.014.

[12] S.E. Day, M.I. Kettunen, F.A. Gallagher, E.-E. Hu, M. Lerche, J. Wolber, K. Golman, J.-H. Ardenkjaer-Larsen, K.M. Brindle, Detecting tumor response to treatment using hyperpolarized $^{13}C$ magnetic resonance imaging and spectroscopy, Nat. Med. 13 (2007) 11, https://doi.org/10.1038/nm1650.

[13] S.J. Nelson, J. Kurhanewicz, D.B. Vigneron, P.E. Z Larson, A.L. Harzstark, M. Ferrone, M. Van Criekinge, J.W. Chang, R. Bok, I. Park, G. Reed, L. Carvaljal, E. J. Small, P. Munster, V.K. Weinberg, J.-H. Ardenkjaer-Larsen, A.p. Chen, R.E. Hurd, L.-I. Odegardstuen, F.J. Robb, J. Tropp, J.A. Murray, Metabolic imaging of patients with prostate cancer using hyperpolarized [1-$^{13}C$]pyruvate, Sci. Transl. Med. 5 (108) (2013) 198, https://doi.org/10.1126/scitranslmed.3006070.

[14] J.T. Grist, M.A. McLean, F. Riemer, R.F. Schulte, S.S. Deen, F. Zaccagna, R. Woitek, C.J. Daniels, J.D. Kaggie, T. Matys, I. Patterson, R. Slough, A.B. Gill, A. Chharbra, R. Eichenberger, M.-C. Laurent, A. Comment, J.H. Gillard, A.J. Coles, D.J. Tyler, I. Wilkinson, B. Basu, D.J. Lomas, M.J. Graves, K.M. Brindle, F.A. Gallagher, Quantifying normal human brain metabolism using hyperpolarized [1-$^{13}C$] pyruvate and magnetic resonance imaging, Neuroimage 189 (2019) 171–179, https://doi.org/10.1016/j.neuroimage.2019.01.027.

[15] J. Kurhanewicz, D.B. Vigneron, J.-H. Ardenkjaer-Larsen, J.A. Bankson, K. M. Brindle, C.H. Cunningham, F.A. Gallagher, K.R. Keshari, A. Kjaer, C. Laustsen, D.A. Mankoff, M.E. Merritt, S.J. Nelson, J.M. Pauly, P. Lee, S. Ronen, D.J. Tyler, S. S. Rajan, D.M. Spielman, L. Wald, X. Zhang, C.r. Malloy, R. Rizi, Hyperpolarized $^{13}C$ MRI: path to clinical translation in oncology, Neoplasia 21 (1) (2019) 1–16, https://doi.org/10.1016/j.neo.2018.09.006.

[16] G.A.N. Gowda, D. Raftery, Biomarker discovery and translation in metabolomics, Curr. Metabolomics 1 (3) (2013) 227–240, https://doi.org/10.2174/2213235X113019990005.

[17] K. Bingol, R. Brüschweiler, Multidimensional approaches to NMR-based metabolomics, Anal. Chem. 86 (2014) 47–57, https://doi.org/10.1021/ac403520j.

[18] P. Giraudeau, Challenges and perspectives in quantitative NMR, Magn. Reson. Chem. 55 (2016) 61–69, https://doi.org/10.1002/mrc.4475.

[19] J.-N. Dumez, J. Milani, B. Vuichoud, A. Bornet, J. Lalande-Martin, I. Tea, M. Yon, M. Maucourt, C. Deborde, A. Moing, L. Frydman, G. Bodenhausen, S. Jannin, P. Giraudeau, Hyperpolarized NMR of plant and cancer cell extracts at natural abundance, Analyst 140 (2015) 5860–5863, https://doi.org/10.1039/C5AN01203A.

[20] A. Bornet, M. Maucourt, c. Deborde, D. Jacob, J. Milani, B. Vuichoud, X. Ji, J.-N. Dumez, A. Moing, G. Bodenhausen, S. Jannin, P. Giraudeau, Highly repeatable dissolution dynamic nuclear polarization for heteronuclear NMR metabolomics, Anal. Chem. 88 (2016) 6179–6183, https://doi.org/10.1021/acs.analchem.6b01094.

[21] N. Hemkens, N. Eshuis, B.J.A. van Weerdenburg, M.C. Feiters, F.P.J.T. Rutjes, S. S. Wijmenga, M. Tessari, NMR-based chemosensing via p-$H_2$ hyperpolarization: application to natural extracts, Anal. Chem. 88 (2016) 3406–3412, https://doi.org/10.1021/acs.analchem.6b00184.

[22] A. Dey, B. Charrier, E. Martineau, C. Deborde, E. Gandriau, A. Moing, D. Jacob, D. Eshchenko, M. Schnell, R. Malzi, D. Kurzbach, M. Ceillier, Q. Chappuis, S. F. Cousin, J.G. Kempf, S. Jannin, J.-N. Dumez, P. Giraudeau, Hyperpolarized NMR metabolomics at natural $^{13}C$ abundance, Anal. Chem. 92 (2020) 14867–14871, https://doi.org/10.1021/acs.analchem.0c03510.

[23] M.H. Lerche, D. Yigit, A.B. Frahm, J.-H. Ardenkjær-Larsen, R.M. Malinowski, P. R. Jensen, Stable isotope-resolved analysis with quantitative dissolution dynamic nuclear polarization, Anal. Chem. 90 (2018) 674–678, https://doi.org/10.1021/acs.analchem.7b02779.

[24] A.B. Frahm, P.R. Jensen, J.-H. Ardenkjær-Larsen, D. Yigit, M.H. Lerche, Stable isotope resolved metabolomics classification of prostate cancer cells using hyperpolarized NMR data, JMR (J. Mol. Recognit.) 316 (2020) 106750, https://doi.org/10.1016/j.jmr.2020.106750.

[25] Clinicaltrials.gov.

[26] H.-Y. Chen, R. Aggarwal, R.A. Bok, M.A. Ohliger, Z. Zhu, P. Lee, J.W. Gordon, M. Van Criekinge, L. Carvajal, J.B. Slater, P.E.Z. Larson, E.J. Small, J. Kurhanewicz, D.B. Vigneron, Hyperpolarized $^{13}C$-pyruvate MRI detects real-time metabolic flux in prostate cancer metastases to bone and liver: a clinical feasibility study, Prostate Cancer Prostatic Dis. 23 (2020) 269–276, https://doi.org/10.1038/s41391-019-0180-z.

[27] N.M. Greensberg, F. Demayo, M.J. Finegold, D. Medina, W.D. Tilley, J.O. Aspinalls, G.R. Cunha, A.A. Donjacour, R.J. Matusik, J.M. Rosen, Prostate cancer in a transgenic mouse, Proc. Natl. Acad. Sci. Unit. States Am. 92 (1995) 3439–3443, https://doi.org/10.1073/pnas.92.8.3439.

[28] J.R. Gingrich, R.J. Barrios, B.A. Foster, N.M. Greenberg, Pathologic progression of autochthonous prostate cancer in the TRAMP model, Prostate Cancer Prostatic Dis. 2 (1999) 70–75, https://doi.org/10.1038/sj.pcan.4500296.

[29] A.A. Hurwitz, B.A. Foster, J.P. Allison, N.M. Greenberg, E.D. Kwon, Curr. The TRAMP mouse as a model for prostate cancer, Protocols in Immun. 20 (5) (2001) 1–23, https://doi.org/10.1002/0471142735.im2005s45.

[30] M.J. Albers, R. Bok, A.P. Chen, C.H. Cunninghamm, M.L. Zierhus, V.Y. Zhang, S. J. Kohler, J. Tropp, R.E. Hurd, Y.-F. Yen, S.J. Nelson, D.B. Vigneron, J. Kurhanewicz, Hyperpolarized $^{13}C$ lactate, pyruvate, and alanine: noninvasive biomarkers for prostate cancer detection and grading, Canc. Res. 68 (2008) 20, https://doi.org/10.1158/0008-5472.CAN-08-0749.

[31] R. Bok, J. Lee, R. Sriram, K. Keshari, S. Sukumar, S. Daneshmandi, D.E. Korenchan, R.R. Flavell, D.B. Vigneron, J. Kurhanewicz, The role of lactate metabolism in prostate cancer progression and metastases revealed by dual-agent hyperpolarized $^{13}C$ MRSI, Cancers 11 (2019) 257, https://doi.org/10.3390/cancers11020257.

[32] D.K. Hill, E. Kim, J.R. Teruel, Y. Jamin, M. Widerøe, C.D. Søgaard, Ø. Størkersen, D. N. Rodrigues, A. Heindl, Y. Yuan, T.F. Bathen, S.A. Moestue, Diffusion-weighted MRI for early detection and characterization of prostate cancer in the transgenic adenocarcinoma of the mouse prostate model, J. magn. Reson. Imaging 43 (2016) 1207–1217, https://doi.org/10.1002/jmri.25087.

[33] S.-M.T. Fagerland, D.K. Hill, A. v-Wamel, C. d-L. Davies, J. Kim, Ultrasound and magnetic resonance imaging for group stratification and treatment monitoring in the transgenic adenocarcinoma of the mouse prostate model, Prostate 80 (2020) 186–197, https://doi.org/10.1002/pros.23930.

[34] T. Chiaverotti, S.S. Couto, A. Donjacour, J.-H. Mao, H. Nagase, R.D. Cardiff, G. R. Cunha, A. Balmain, Dissociation of epithelial and neuroendocrine carcinoma lineages in the transgenic adenocarcinoma of mouse prostate model of prostate

cancer, Am. J. Pathol. 172 (2008) 236–246, https://doi.org/10.2353/ajpath.2008.070602.
[35] H.U. Bergmeyer (Ed.), Methods of Enzymatic Analysis, Verlag Chemie, Weinheim, 1983.
[36] S. Katsikis, I. Marin-Montesinos, M. Pons, C. Ludwig, U.L. Günther, Improved stability and spectral quality in ex situ dissolution DNP using an improved transfer device, Appl. Magn. Reson. 46 (2015) 723–729, https://doi.org/10.1007/s00723-015-0680-5.
[37] MNova Version 11.0; MestreLab Research.
[38] MATLAB, Version 9.6.0, The MathWorks Inc, Natick, Massachusetts, 2019. R2019a.
[39] F. Savorani, G. Tomasi, S.B. Engelsen, Icoshift: a versatile tool for the rapid alignment of 1D NMR spectra, J. Magn. Reson. 202 (2010) 190–202, https://doi.org/10.1016/j.jmr.2009.11.012.
[40] D.S. Wishart, Y.D. Feunang, A. Marcu, A.C. Guo, K. Liang, et al., The human metabolome database for 2018, Nucleic Acids Res. 46 (D1) (2018) D608–D617, https://doi.org/10.1093/nar/gkx1089.
[41] Python Software Foundation, Python language reference, version 3. Available at: http://www.python.org.
[42] F. Pedregosa, G. Varoquaux, A. Gramfort, V. Michel, B. Thirion, O. Grisel, E. Duchesnay, Scikit-learn: machine learning in {P}ython, J. Mach. Learn. Res. 12 (2011) 2825–2830.
[43] E. Jones, T. Oliphant, P. Peterson, & others. (n.d.). {SciPy}: Open-source scientific tools for {Python}. Retrieved from, http://www.scipy.org/.
[44] S. Meier, M. Karlsson, P.R. Jensen, M.H. Lerche, J.Ø. Duus, Metabolic pathway visualization in living yeast by DNP-NMR, Mol. Biosyst. 7 (2011) 2834–2836, https://doi.org/10.1039/c1mb05202k.
[45] S.P. Wang, D. Zhou, Z. Yao, S. Satapati, Y. Chen, N.A. Daurio, A. Petrov, X. Shen, D. Metz, D.E. Kelley, Quantifying rates of glucose production in vivo following an intraperitoneal tracer bolus, Am. J. Physiol. Endocrinol. Metab. 311 (2016) E911–E921, https://doi.org/10.1152/ajpendo.00182.2016.
[46] A. Lane, J. Yan, T.W.-M. Fan, $^{13}$C tracer studies of metabolism in mouse tumor xenografts, Bio Protoc 5 (2015) 22, https://doi.org/10.21769/bioprotoc.1650.
[47] C.X. Hsu, B.D. Ross, C.E. Chrisp, S.Z. Derrow, L.G. Charlse, K.J. Pienta, N. M. Greenberg, Z. Zeng, M.G. Sanda, Longitudinal cohort analysis of lethal prostate cancer progression in transgenic mice, J. Urol. 160 (1998) 1500–1505, https://doi.org/10.1016/S0022-5347(01)62603-X.
[48] S. Bowen, C. Hilty, Phys. Rapid sample injection for hyperpolarized NMR spectroscopy, Chem. Chem. Phys. 12 (2010) 5766–5770, https://doi.org/10.1039/C002316G.
[49] S. Jannin, A. Bornet, R. Melzi, G. Bodenhausen, High field dynamic nuclear polarization at 6.7 T: Carnon-13 polarization above 70% within 20 min, Chem. Phys. Lett. 549 (2012) 99–102, https://doi.org/10.1016/j.cplett.2012.08.017.
[50] J.H. Ardenkjær-Larsen, S. Bowen, J.R. Petersen, O. Rybalko, M.S. Vinding, M. Ullisch, N.C. Nielsen, Cryogen-free dissolution dynamic nuclear polarization polarizer operating at 3.35 T, 6.7 T and 10.1 T, Magn. Reson. Med. 81 (2019) 2184–2194, https://doi.org/10.1002/mrm.27537.
[51] T. Cheng, A.P. Gaunt, I. Marco-Ruis, M. Gehrung, A.P. Chen, J.J. Klink, A. Comment, A multisample 7 T dynamic nuclear polarization polarizer for preclinical hyperpolarized MR, NMR Biomed. 33 (2020) 1–10, https://doi.org/10.1002/nbm.4264.
[52] M. Baudin, B. Vuichoud, A. Bornet, G. Bodenhausen, S. Jannin, A cryogen-free system for dynamic nuclear polarization at 9.4 T, J. Magn. Reson. 294 (2018) 115–121, https://doi.org/10.1016/j.jmr.2018.07.001.
[53] V. Gialleonardo, S.S. Tee, H.N. Aldeborgh, V.Z. Miloushev, L.S. Cunha, G. D. Sukenick, K.R. Keshari, High-throughput indirect quantitation of $^{13}$C enriched metabolites using $^{1}$H NMR, Anal. Chem. 88 (2016) 11147–11153, https://doi.org/10.1021/acs.analchem.6b03307.
[54] N. Krause, A. Wegner, Fructose metabolism in cancer, Cells 9 (2020) 2635, https://doi.org/10.3390/cells9122635.
[55] A. Godoy, V. Ulloa, F. Rodriguez, K. Reinicke, A.J. Yanez, M. Garcia, R.A. Medina, M. Carrasco, S. Barberis, R. Nualart, Differential subcellular distribution of glucose transporters GLUT1–6 and GLUT9 in human cancer: ultrastructural localization of GLUT1 and GLUT5 in breast tumor tissues, J. cell. Phys. 207 (2006) 614–627, https://doi.org/10.1002/jcp.20606.
[56] A. Andres-Hernando, R.J. Johnson, M.A. Lanaspa, Endogenous fructose production: what do we know and how relevant is it? Curr. Opin. Clin. Nutr. Metab. Care 22 (4) (2019) 289–294, https://doi.org/10.1097/MCO.0000000000000573.
[57] K. Reinicke, P. Sotomayor, P. Cisterna, C. Delgado, F. Nualart, A. Godoy, Cellular distribution of Glut-1 and Glut-5 in benign and malignant human prostate tissue, J. Cell. Biochem. 113 (2012) 553–562, https://doi.org/10.1002/jcb.23379.
[58] K.R. Keshari, D.M. Wilson, A.P. Chen, R. Bok, P.E.Z. Larson, S. Hu, M.V. Criekinge, J.M. Macdonald, D.B. Vigneron, J. Kurhanewicz, Hyperpolarized [2-$^{13}$C]-Fructose: a hemiketal DNP substrate for in vivo metabolic imaging, JACS 131 (2009) 17591–17596, https://doi.org/10.1021/ja9049355.
[59] A.R. Lima, J. Pinto, F. Amaro, M.d.L. Bastos, M. Carvalho, P. Guedes de Pinho, Advances and perspectives in prostate cancer biomarker discovery in the last 5 years through tissue and urine metabolomics, Metabolites 11 (3) (2021) 181, https://doi.org/10.3390/metabo11030181.
[60] C. Canepè, G. Catanzaro, E. Terreno, M. Karlsson, M.H. Lerche, P.R. Jensen, Probing treatment response of glutaminolytic prostate cancer cells to natural drugs with hyperpolarized [5-13C]glutamine: glutaminolysis to measure drug response in cancer cells, MRM 73 (6) (2015) 2296–2305, https://doi.org/10.1002/mrm.25360.
[61] M. Ragavan, M.A. McLeod, A.G. Giacalone, M. Merritt, Hyperpolarized dihydroxyacetone is a sensitive probe of hepatic gluconeogenic state, Metabolites 11 (2021) 441, https://doi.org/10.3390/metabo11070441.